Molecular Therapy
Oncolytics
Original Article

Generation of a Tumor-Specific Chemokine Gradient Using Oncolytic Vesicular Stomatitis Virus Encoding CXCL9

Elizabeth C. Eckert,[1,2] Rebecca A. Nace,[1] Jason M. Tonne,[1] Laura Evgin,[1] Richard G. Vile,[1] and Stephen J. Russell[1]

[1]Department of Molecular Medicine, Mayo Clinic, Rochester, MN 55905, USA; [2]Clinical and Translational Science Track, Mayo Graduate School of Biomedical Science, Mayo Clinic, Rochester, MN 55905, USA

Genetically modified vesicular stomatitis virus (VSV) is an attractive agent for cancer treatment due to rapid intratumoral replication and observed clinical responses. Although VSV selectively kills malignant cells and can boost antitumor immunity, limited induction of intratumoral immune infiltration remains a barrier to efficacy in some cancer models. Here we engineered the oncolytic VSV platform to encode the T cell chemokine CXCL9, which is known to mediate the recruitment of activated $CD8^+$ cytotoxic T cells and $CD4^+$ T helper cells, and demonstrates conserved protein function between mice and humans. Chemotactic activity of the virally encoded chemokine was confirmed *in vitro*. Intratumoral concentration of CXCL9 was shown to increase after VSV therapy in three different cancer models, but to a much greater degree after VSV-CXCL9 therapy as compared with VSV control viruses. Despite a steep chemokine gradient from the tumor to the bloodstream, tumor trafficking of adoptively transferred and endogenous T cells was not measurably increased following VSV-CXCL9 therapy. Our results indicate that oncolytic VSV infection promotes release of CXCL9 in the tumor microenvironment, but further boosting of the functional chemokine gradient through virus engineering has little incremental impact on intratumoral immune cell infiltration in mouse and human tumor models.

INTRODUCTION

Chemokines are chemotactic cytokines that orchestrate immune cell migration throughout the body. Chemokine structural classification is based on the number and position of conserved cysteine residues on the N terminus of the proteins into C, CC, CXC, or CXC3C groups, whereas function is based on their ability to direct cell positioning in the body.[1] Homeostatic chemokine expression is necessary for recruitment of naive immune cells into the lymph nodes, and inflammatory chemokine expression occurs transiently in response to an injury or infection.[1] Chemokines bind seven-transmembrane G protein-coupled receptors (GPCRs) that subsequently signal migration, proliferation, cell survival, or a combination of these effects.[1]

Chemokines may therefore be an important factor aiding the recruitment of T cells and other immune cells into the tumor microenvironment. Tumors have been shown to down-modulate chemokines that support immune cell infiltration via expression of chemokine-cleaving proteases or through epigenetic silencing.[2–8] Restoring the intratumoral expression of chemokines that are consistently downregulated may therefore prove therapeutically advantageous.

Oncolytic virotherapy uses replication-competent viruses to specifically replicate in and kill tumor cells, while leaving normal cells unharmed.[9] Vesicular stomatitis virus (VSV) is a rhabdovirus belonging to the genus *Vesiculovirus* with a negative sense, single-stranded RNA genome and a rapid replication cycle.[10] Antitumor activity of VSV has been demonstrated in numerous mouse tumor models, in pet dogs with spontaneous tumors, and in early-phase clinical trials.[11–14] The efficacy of VSV depends to varying degrees on the two phases of killing: an oncolytic phase where the virus propagates selectively in tumor cells killing them directly, and an immune phase during which the immune system continues to kill uninfected tumor cells after the virus has been cleared. VSV efficacy is compromised in certain tumor models because of poor transitioning from the oncolytic phase to the immunotherapeutic phase, resulting in insufficient immune cell infiltration to the tumor.[11,15] VSV is often cleared rapidly from the host, rendering it unable to efficiently recruit antitumor T cells back to the tumor, potentially limiting its efficacy.

CXCR3 ligands, CXCL9, CXCL10, and CXCL11, have been shown to limit tumor progression by attracting antitumor cytotoxic T lymphocytes (CTLs) to the tumor.[16–23] CXCL9 offers theoretical advantages over CXCL10 and CXCL11 as an antitumor chemokine. In contrast with CXCL11, which attracts both cytotoxic and regulatory T cells, CXCL9 primarily attracts $CD8^+$ cytotoxic T cells.[24] Compared with CXCL10, CXCL9 has equivalent activity and specificity, but CXCL10 is preferentially cleaved by the CD26 peptidase, presumably shortening the *in vivo* half-life.[2,4] CXCL9 has an extended COOH-terminal domain that binds to glycosaminoglycans (GAGs), thereby anchoring the protein in the extracellular matrix and creating a

Received 30 September 2019; accepted 7 December 2019;
https://doi.org/10.1016/j.omto.2019.12.003.

Correspondence: Stephen J. Russell, Department of Molecular Medicine, Mayo Clinic, 200 First Street SW, Guggenheim 1833, Rochester, MN 55905, USA.
E-mail: sjr@mayo.edu

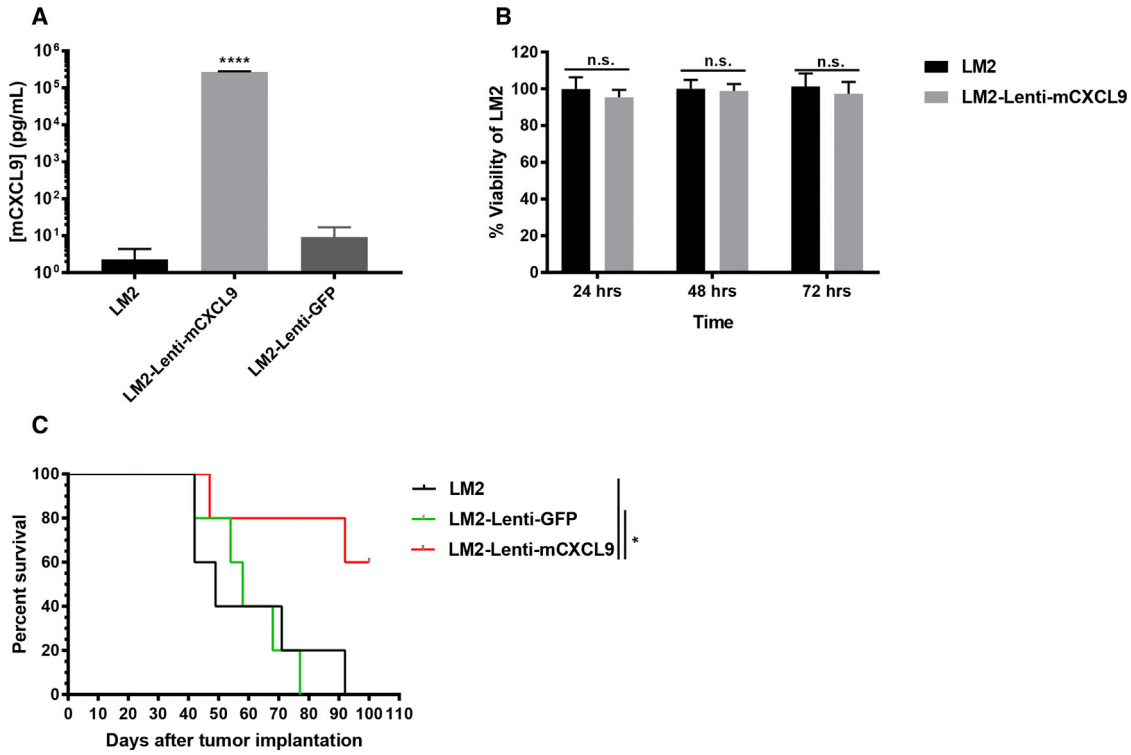

Figure 1. LM2 Cells Transduced with Lenti-mCXCL9 Have Reduced Tumorigenicity *In Vivo* Compared with LM2

(A) Concentration of mCXCL9 levels in the supernatants of LM2 cells transduced with Lenti-mCXCL9. ELISA data are shown at 24 h after plating in triplicate + standard deviation (****$p < 0.0001$). (B) Viability of LM2-Lenti-mCXCL9 compared with LM2 cells *in vitro*. Data are shown as mean percent cell viability in comparison with mock-infected cells at 24, 48, and 72 h postinfection + standard deviation. (C) Survival of mice bearing LM2 or Lenti-transduced LM2 tumors was evaluated using Kaplan-Meier survival curves (*$p < 0.05$).

chemokine gradient between the tissue and the bloodstream.[25,26] Several studies have shown increased CXCL9 transcript or protein levels in colorectal cancer and their correlation with improved survival.[18,27] In light of these observations, we engineered the CXCL9 coding sequence into an oncolytic VSV backbone and explored the effect of delivering CXCL9 to the tumor in the context of an oncolytic infection in mouse cancer models.

RESULTS

Tumorigenicity of LM2 Cells Expressing Murine CXCL9

Murine LM2 non-small cell lung cancer cells were transduced with lentiviruses encoding murine CXCL9 (mCXCL9) or green fluorescent protein (GFP). CXCL9 ELISA confirmed a high concentration of mCXCL9 in supernatants harvested from the Lenti-mCXCL9-transduced cells compared with control Lenti-GFP-transduced cells (Figure 1A). 3-(4, 5-Dimethylthiazolyl-2)-2, 5-diphenyltetrazolium bromide (MTT) assays confirmed that there was no impact of mCXCL9 expression on LM2 cell viability compared with control cells (Figure 1B). Tumorigenicity of mCXCL9-expressing and control LM2 tumor cells was compared after subcutaneous implantation in A/J mice. As shown in Figure 1C, tumor cells expressing mCXCL9 showed significantly impaired tumorigenicity compared with control LM2 cells, characterized by slowed tumor growth and prolonged survival (Figure 1C).

Oncolytic VSVs Encoding CXCL9

VSV consists of five genes, the nucleocapsid (N), phosphoprotein (P), matrix (M), glycoprotein (G), and large protein (L) genes. mCXCL9, murine CXCL inactive (mCXCLi), and GFP genes were engineered in the VSV backbone between the G and L genes (Figure 2A). mCXCLi is a biologically inactive form of mCXCL9, derived by deleting a portion of the receptor binding domain, rendering the protein unable to bind and signal through the CXCR3 receptor. VSVs encoding human CXCL9 (hCXCL9) and human CXCLi (hCXCLi) were also constructed using a modified VSV backbone containing a matrix inactivating mutation (M51R) (Figure 2B). VSVs incorporating M51R or related matrix mutations are defective in their ability to suppress the innate antiviral responses of infected target cells, potentially increasing their immunogenicity.[28]

Recombinant VSVs were rescued using an established reverse genetics system, and multi-step viral growth kinetics were tested in African Green Monkey kidney epithelial (Vero) cells (Figure 2C).[9] Insertion of the *mcxcl9*, *mcxcli*, *hcxcl9*, and *hcxcli* transgenes

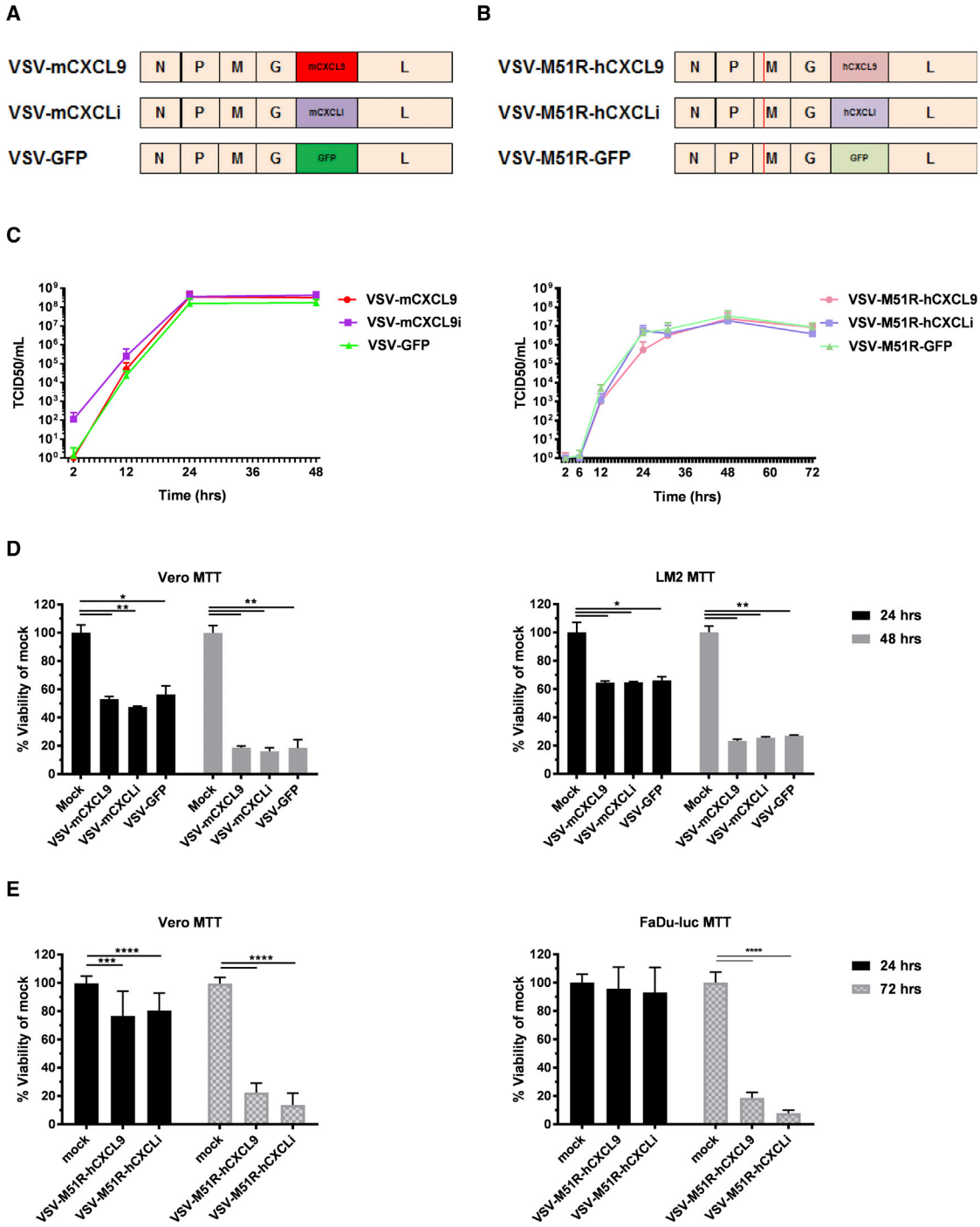

Figure 2. Murine and Human CXCL9 Transgenes Engineered in Recombinant VSVs Do Not Alter the Growth Kinetics or Viral Killing Ability *In Vitro*

Schematic depiction of the genomes of recombinant VSVs encoding murine (A) or human (B) CXCL9, CXCLi, and GFP. (C) Replication kinetics of VSVs encoding murine or human CXCL9 were performed in a multistep viral growth curve in Vero cells. Data are shown from duplicate experiments as average titer + standard deviation. (D) Viability of VSV-mCXCL9-, VSV-mCXCLi-, and VSV-GFP-infected Vero and murine LM2 tumor cells was assessed at 24 and 48 h postinfection at an MOI of 10. (E) Viability of VSV-M51R-hCXCL9- and VSV-M51R-hCXCLi-infected Vero and human FaDu-Luc tumor cells was measured at 24 and 72 h postinfection at an MOI of 10. Data are presented as duplicate experiments as average percent viability compared with mock-infected cells + standard deviation. Significance was determined by paired t test (*$p < 0.05$, **$p < 0.01$, ***$p < 0.001$, ****$p < 0.0001$).

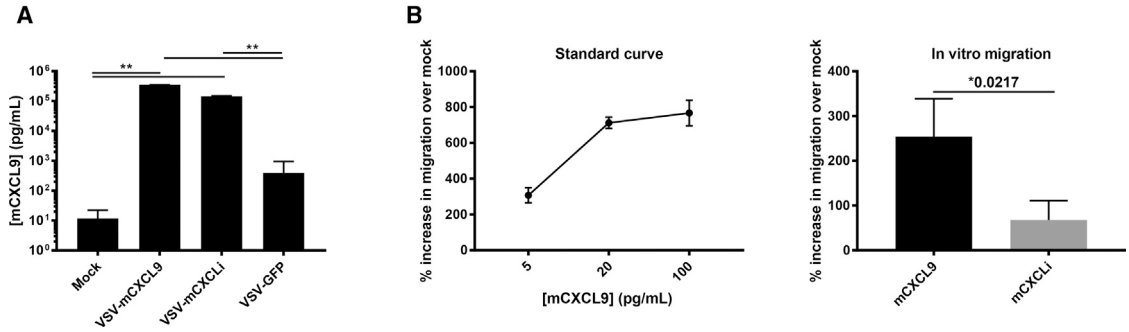

Figure 3. CXCL9 Expressed from VSV-mCXCL9 Is Biologically Active

(A) Murine CXCL9 secretion was evaluated *in vitro* in the LM2 non-small cell lung cancer cell line. Supernatants of VSV-infected LM2 cells (MOI 0.1) were collected 24 h postinfection, and chemokine concentration was determined by ELISA. Concentrations are presented as average concentration + standard deviation. (B) Chemotactic activity of virally encoded mCXCL9 was assessed in an *in vitro* migration assay adapted from Campanella et al.[29] Numbers of migrated cells are presented as average percent increase in migration compared with mock treated + standard deviation. Significance was determined by paired two-tailed t test (**$p < 0.01$).

had no impact on virus replication kinetics compared with corresponding (wild-type matrix gene or M51R) parental viruses carrying the GFP transgene. Oncolytic activity of the recombinant VSVs encoding mCXCL9 and mCXCLi was not discernably decreased compared with VSV-GFP in Vero and LM2 cells (Figure 2D). Likewise, the oncolytic activities of VSV-M51R-hCXCL9 and VSV-M51R-hCXCLi were found to be equivalent in Vero and FaDu-Luc (human head and neck squamous cell carcinoma) cells compared with mock (Figure 2E).

Chemotactic Activity of Virally Encoded mCXCL9

Supernatants of LM2 cells were collected 24 h postinfection with VSV-mCXCL9, VSV-mCXCLi, VSV-GFP, or mock infection at an MOI of 0.1, and mCXCL9 protein concentrations were quantified by ELISA (Figure 3A). Interestingly, infection with the control VSV-GFP virus resulted in a ~50-fold increase in the supernatant concentration of mCXCL9. However, infection with VSV-mCXCL9 (and with VSV-mCXCLi) resulted in a ~10,000-fold increase in the supernatant concentration of immunoreactive mCXCL9. Biological activity of the virally encoded mCXCL9 (and inactivity of the virally encoded mCXCL9i) in supernatants from VSV-infected LM2 cells was subsequently confirmed using an established Transwell migration chemotaxis assay (Figure 3B).[29] Diluted supernatants from VSV-mCXCL9-infected LM2 cells resulted in a significant increase in OT-1 cell migration compared with supernatants from VSV-mCXCLi-infected cells.

Antitumor Activity of VSV-mCXCL9

We compared the antitumor activity of VSV-mCXCL9 and VSV-GFP in syngeneic 5TGM1 (plasmacytoma) and LM2 (NSCLC) tumor models. Mice bearing established subcutaneous 5TGM1 tumors received a single intravenous dose of 5×10^7 tissue culture infectious dose 50 ($TCID_{50}$) of VSV-mCXCL9 or VSV-GFP, leading to significant retardation of tumor growth and prolongation of survival compared with the PBS control group, which was equivalent for both viruses (Figure 4A). Subsequently, A/J mice with established subcutaneous LM2 tumors were injected intratumorally with 5×10^8 $TCID_{50}$ of virus. Neither VSV-mCXCL9 nor VSV-GFP improved survival compared with PBS-treated mice (Figure 4B).

Tumor to Blood Chemokine Gradients in VSV-Treated Mice

We next sought to determine whether VSVs encoding CXCL9 could establish a meaningful chemokine gradient between the interstitial compartment of the virus-infected tumor and the bloodstream. LM2 tumors were injected with 5×10^8 $TCID_{50}$ VSV-mCXCL9, VSV-GFP, or PBS and harvested at 24 or 96 h post virus administration for processing and quantification of the interstitial fluid concentration of mCXCL9. The interstitial concentration of mCXCL9 was 10-fold higher in VSV-mCXCL9-injected tumors compared with PBS-injected tumors 24 h post virus administration, but had returned to baseline by 96 h (Figure 5). Interestingly, the intratumoral concentration of mCXCL9 was increased 2-fold above PBS control in tumors injected with VSV-GFP, consistent with our *in vitro* studies demonstrating release of mCXCL9 by VSV-GFP-infected LM2 cells (Figure 3A).

To determine whether local production of the virally encoded chemokine could generate an increased chemokine gradient between tumor and blood, we also determined serum mCXCL9 concentrations in the virus-injected mice at the 24- and 96-h time points and compared them with the intratumoral concentrations. mCXCL9 serum concentrations of VSV-mCXCL9- and VSV-GFP-injected mice were significantly increased at the 24-h time point compared with PBS-injected mice, creating a steep tumor to serum CXCL9 chemokine concentration gradient, especially in the VSV-mCXCL9-injected animals (Figure 5). An even steeper mCXCL9 chemokine gradient was observed in mice bearing syngeneic murine plasmacytoma cell (MPC-11) murine plasmacytomas after systemic administration of VSV-mCXCL9 (data not shown). These data demonstrate that a steep blood to tumor mCXCL9 gradient is generated in the LM2 tumor model 24 h post VSV-mCXCL9 injection but also point to a lesser mCXCL9 gradient after injection of the control virus (VSV-GFP).

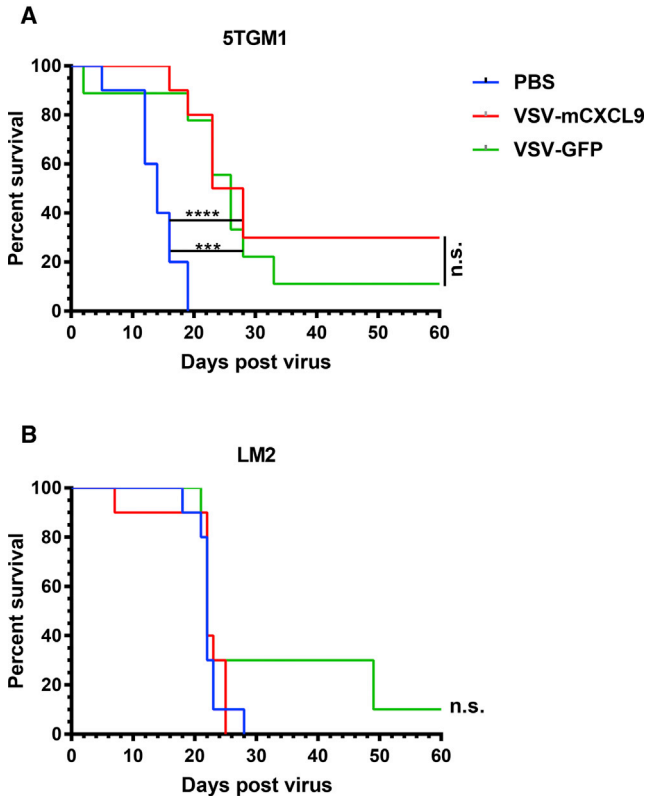

Figure 4. Oncolytic Activity of VSV-mCXCL9

Survival of mice bearing 5TGM1 or LM2 tumors was evaluated using Kaplan-Meier survival curves. (A) 5×10^6 5TGM1 cells were implanted subcutaneously on the right flanks of C57Bl6/KaLwRij mice; once tumors had grown to ~6-mm diameter, mice were injected intravenously with PBS, VSV-mCXCL9, or VSV-GFP (n = 10 for PBS and VSV-mCXCL9 treatments, n = 9 for VSV-GFP treatment). (B) 1×10^6 LM2 cells were implanted subcutaneously on the right flanks of A/J mice, and established tumors (~6-mm diameter) were injected intratumorally with PBS, VSV-mCXCL9, or VSV-GFP (n = 10 for all treatment groups). Survival analysis was performed using log rank statistics (***$p < 0.001$, ****$p < 0.0001$).

Increasing Tumor to Blood CXCL9 Chemokine Gradient Does Not Impact T Cell Infiltration

Multicolor flow cytometry of dissociated tumors was used to quantify intratumoral T cell infiltration in LM2 tumor-bearing mice 7 or 10 days after intratumoral injection of VSV-mCXCL9, VSV-GFP, or PBS. Although both viruses were associated with a small increase in the intratumoral influx of $CD8^+$ T cells on day 10 post virus administration, VSV-mCXCL9 did not measurably increase intratumoral T cell infiltration compared with VSV-GFP (Figures 6A and 6C). We next tested the interferon gamma (IFN-γ) and tumor necrosis factor alpha (TNF-α) cytokine production from tumor-infiltrating $CD8^+$ T cells as a measure of T cell reactivity within the tumor. Whereas cytokine production from intratumoral $CD8^+$ T cells in VSV-GFP-treated mice trended toward higher levels at day 10 post virus administration, there was no increase in cytokine production from the T cells extracted from VSV-mCXCL9-injected tumors (Figure 6B).

VSV-M51R-hCXCL9 Did Not Improve Recruitment of Adoptively Transferred Human T Cells into FaDu-Luc Xenografts

To determine whether T cell recruitment might be transiently enhanced during the first 24–48 h after administering a CXCL9-encoding VSV, coincident with the timing of the peak tumor to blood chemokine gradient, we adoptively transferred human T cells to immunodeficient mice bearing human FaDu-Luc tumor xenografts. First, we confirmed an increased concentration of hCXCL9 in FaDu-Luc supernatants following VSV-M51R-hCXCL9 infection *in vitro* (Figure 7A). It should be noted in this assay that hCXCLi is not detected by the ELISA we used for detection of the full-length hCXCL9, and the low levels of CXCL9 detected in supernatants from VSV-M51R-hCXCLi supernatants are likely due to induction of endogenous CXCL9 expression from the infected cells. Subsequently, we confirmed that intratumoral administration of VSV-M51R-hCXCL9 could generate a steep tumor to blood CXCL9 chemokine gradient in FaDu-Luc tumor xenografts *in vivo*. The tumor hCXCL9 concentration was logarithmically increased in VSV-M51R-hCXCL9-treated mice compared with VSV-M51R-hCXCLi and PBS controls at all time points, generating a steep tumor to blood chemokine gradient with intratumoral concentrations approximately 100-fold higher than corresponding plasma concentrations (Figure 7A). In contrast with our observations in the LM2 model (Figure 5), the steep tumor to blood chemokine concentration gradient was maintained for at least 96 h post virus administration in mice bearing FaDu-Luc tumors (Figure 7A).

To assess the recruitment of adoptively transferred T cells into virus-infected FaDu-Luc tumors, we intravenously administered activated $CXCR3^+$ primary human T cells (Figure 7B). Tumors were harvested and processed for quantification of immune cell infiltrates at 24 and 72 h after adoptive cell transfer (48 and 96 h post virus injection). Twenty-four hours after adoptive cell transfer, there were fewer infiltrating immune cells in tumors injected with VSV-M51R-hCXCL9 compared with those injected with VSV-M51R-hCXCLi. By 72 h, both groups of VSV-injected animals showed a significant increase in intratumoral immune cell infiltration compared with the PBS control group. However, T cell infiltration of VSV-M51R-hCXCL9-injected tumors was not increased compared with those injected with VSV-M51R-hCXCLi (Figure 7B).

DISCUSSION

Here we have shown that tumor cells infected with VSVs encoding CXCL9 produce abundant biologically active CXCL9 chemokine. Intratumoral replication and antitumor activity of CXCL9-encoding VSVs were confirmed in tumor-bearing mice, and the virally encoded chemokine expressed from the infected tumors was able to drive a substantial increase in the CXCL9 chemokine gradient between tumor and blood. However, increasing the intratumoral CXCL9 chemokine concentration in this way did not lead to enhanced migration of circulating T cells into the tumor parenchyma in comparison with tumors that had been infected with control viruses.

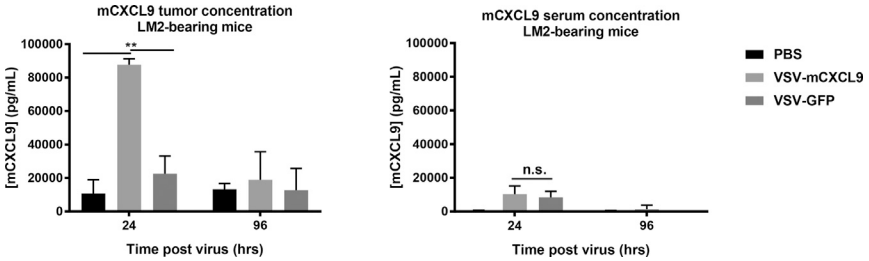

Figure 5. Generation of a Tumor to Blood CXCL9 Chemokine Gradient after Intratumoral VSV-mCXCL9 Administration

Intratumoral and serum mCXCL9 protein concentrations were determined after intratumoral injection of VSV-mCXCL9 or VSV-GFP in LM2 tumor-bearing mice by ELISA (n = 3 mice/group for each time point). Values are presented as average chemokine concentration in pg/mL + standard deviation. Significance was determined by paired two-tailed t test (**$p < 0.01$).

Interestingly, increased intratumoral T cell infiltration was often observed in tumors injected with control viruses not encoding CXCL9, which also generated an increased tumor to blood CXCL9 chemokine concentration, albeit to a far lesser degree than was observed in tumors injected with CXCL9-encoding VSVs. It is therefore possible that inflammatory tumor cell killing by VSV is capable of driving sufficient local release of endogenous T cell-attracting chemokines (CXCL9 and CXCL10) to maximally stimulate the recruitment of these effector cells into the tumor. Additional virus-encoded chemokine may therefore be superfluous to requirements.

VSV-CXCL9-treated LM2 tumors did not regress, whereas LM2 tumor cells overexpressing CXCL9 showed reduced tumorigenicity. This discrepancy is likely a consequence of the limited spread of VSV-CXCL9 in treated tumors and the short duration of intratumoral CXCL9 expression, but may also reflect an unfavorable tumor-to-blood ratio of CXCL9 in virus-infected tumors compared with tumors derived from stably transduced LM2 cells.

In all tumor models tested in this study, virally encoded CXCL9 was locally retained at the site of production, generating intratumoral CXCL9 concentrations at least 10-fold higher than corresponding blood concentrations. Indeed, in some of our experiments, the intratumoral accumulation of T cells in VSV-CXCL9-injected tumors was reduced compared with tumors injected with control VSVs. The possibility therefore arises that massively increased intratumoral release of CXCL9 concentration may negatively impact immune infiltration. At very high intratumoral concentrations of CXCL9, some spillage into the bloodstream was apparent, and it is possible that this circulating CXCL9 may have bound and saturated CXCR3 receptors on circulating T cells, thereby impeding their ability to migrate into the tumor in response to an accentuated chemokine gradient. Alternatively, in some situations, prolonged local chemokine secretion has been shown to cause increased chemokine receptor signaling, T cell hypofunction, and anergy.[30,31] Chemokine receptor signaling increases intracellular calcium levels via phospholipase C, which, over prolonged periods of time, can lead to both hypofunction and anergy, rendering the cells unable to appropriately migrate to the site of inflammation and/or to function upon antigen recognition.

The importance of a physiologically relevant T cell chemokine gradient was previously demonstrated using mesothelin-directed chimeric antigen receptor (CAR) T cells engineered to express CXCL11 (CAR T/CXCL11).[32] Tumor and serum CXCL11 concentrations were increased in mice transfused with CAR T/CXCL11 cells, but intratumoral CAR T cell infiltration and antitumor activity in a mesothelin-positive TC-1 tumor model were inferior compared with non-transduced CAR T. *In vitro* tumor cell killing by CAR T/CXCL11 was decreased 30% compared with parental CAR T cells, supporting the possibility of T cell hypofunction and anergy after prolonged exposure to CXCL11.[32] Decreased functionality of tumor-infiltrating $CD8^+$ T cells was also observed in our study, supporting the possibility that excessive CXCL9 signaling may have resulted in T cell anergy.

An additional factor that may determine the impact of a virally encoded chemokine on intratumoral T cell migration is the immunogenicity of the tumor model. Oncolytic virus (OV) infection and killing of immunogenic tumors may prime a stronger antitumor T cell response that, when effectively trafficked to the tumor, may produce a meaningful enhancement of the antitumor response. We chose the 5TGM1, LM2, and FaDu tumor models based on previous studies showing that these tumors are responsive to immunotherapy, virotherapy, and/or adoptive T cell therapy.[11,15,33–35] In particular, we focused on the LM2 model because of prior published work demonstrating that intratumoral injection of a VSV encoding murine IFN-β led to substantial intratumoral infiltration with $CD8^+$ T cells.[15] We did see a modest increase in intratumoral $CD8^+$ T cells after VSV-GFP infection, but not to the extent that was previously reported using VSV-mIFN-β in this model, suggesting that, compared with CXCL9, IFN-β may be better suited to the purpose of enhancing intratumoral inflammation. However, it remains possible that studies using alternative tumor models might give very different results compared with those reported in this manuscript.

Another factor likely to influence the therapeutic utility of a virally encoded T cell chemokine is the nature of the virus into which it is engineered. OVs derived from a variety of virus families are currently being developed, and several have entered clinical testing.[36] Each OV platform differs from the others in terms of genome size and complexity, replication kinetics, cell-killing mechanism, and ability to control the innate and adaptive host immune responses. In contrast with VSV, which has a simple genome and encodes only five proteins, OVs derived from the Herpesviridae and Poxviridae families have large, complex genomes encoding ~200 proteins, many of which have evolved to interfere with specific components of the host immune and inflammatory responses.[37–40] Thus, the outcome of our studies in the VSV platform cannot necessarily be extrapolated to other OVs. When CXCL11 was engineered into an oncolytic vaccinia

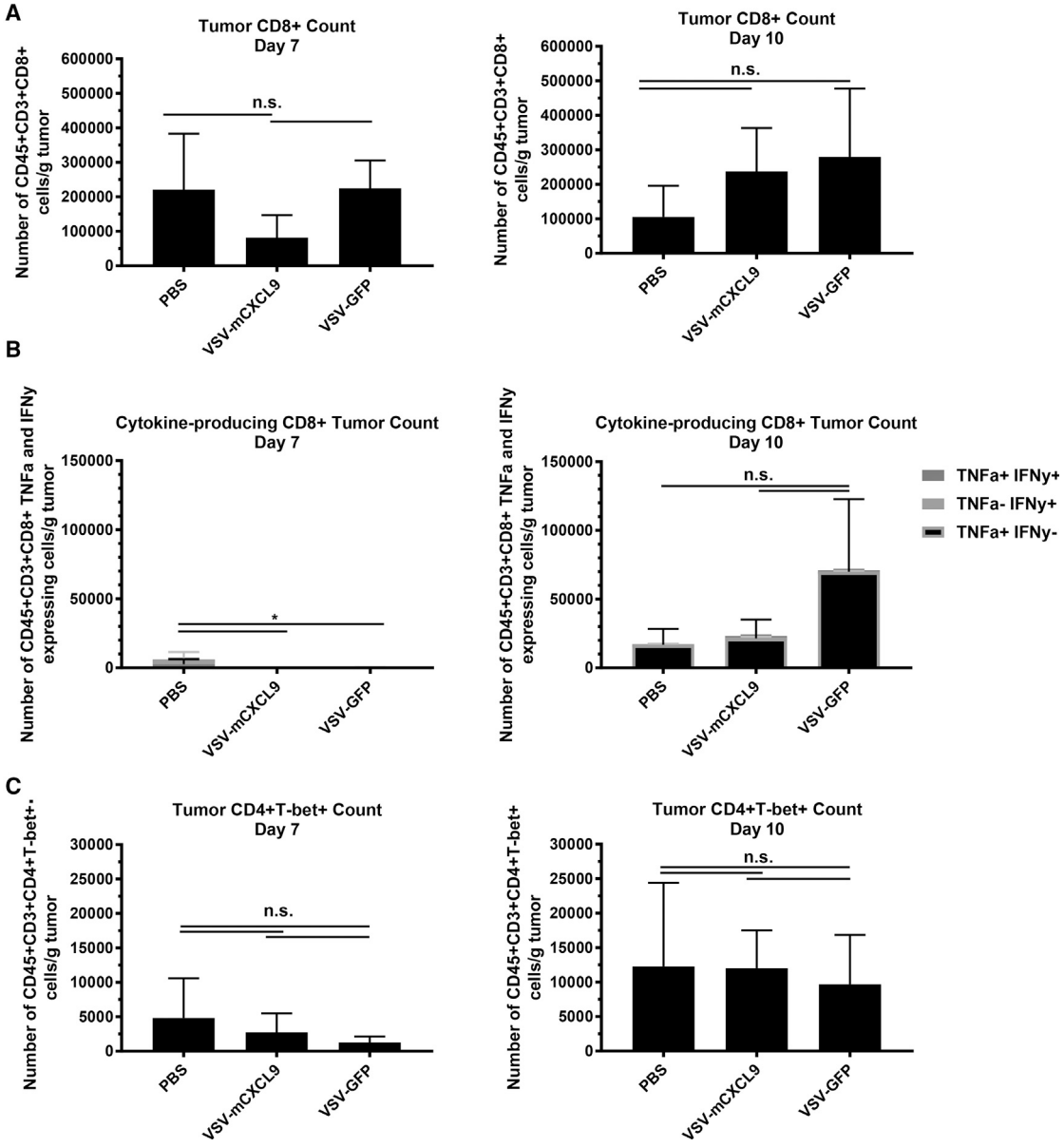

Figure 6. VSV-mCXCL9 Does Not Increase CD8⁺ or Th1 Cell Intratumoral Infiltration or CD8⁺ Inflammatory Cytokine Production

LM2 tumors were harvested and processed 7 and 10 days after intratumoral (i.t.) injection of VSV-mCXCL9, VSV-GFP, or PBS, and flow data were gated on (A) $CD45^+CD3^+CD8^+$ T cells or (C) $CD45^+CD3^+CD4^+$T-bet^+ (Th1) cells. T cell numbers are presented as average number of immune cells/mg tumor ± standard deviation (n = 4 mice/group/day). (B) Cytokine production was gated on TNF-α- and IFN-γ-producing cells from (A). Statistical significance was determined by paired two-tailed t test (*$p < 0.05$).

virus backbone, the resulting virus (VV-CXCL11) was shown not only to generate a tumor-specific chemokine gradient, but also recruit immune cells more efficiently into the tumor parenchyma, sometimes resulting in a significant survival benefit in TC-1, MC38, and AB12 tumor models.[32,41–43] Interestingly, in contrast with our findings with VSV and CXCL9, *in vivo* CXCL11 concentrations were decreased after administration of a control vaccinia virus not expressing CXCL11, suggesting that vaccinia may have evolved to suppress this chemokine, and that the engineering of CXCL11 into the vaccinia backbone is an elegant way to overcome the block.[41]

An area for future investigation is the role that natural killer (NK) cells play in mediating VSV-mCXCL9 replication. It is possible that virally produced CXCL9 recruits NK cells early during infection, kills VSV-infected tumor cells, and limits VSV-mCXCL9 titers, cumulatively reducing efficacy. One strategy to overcome a possible

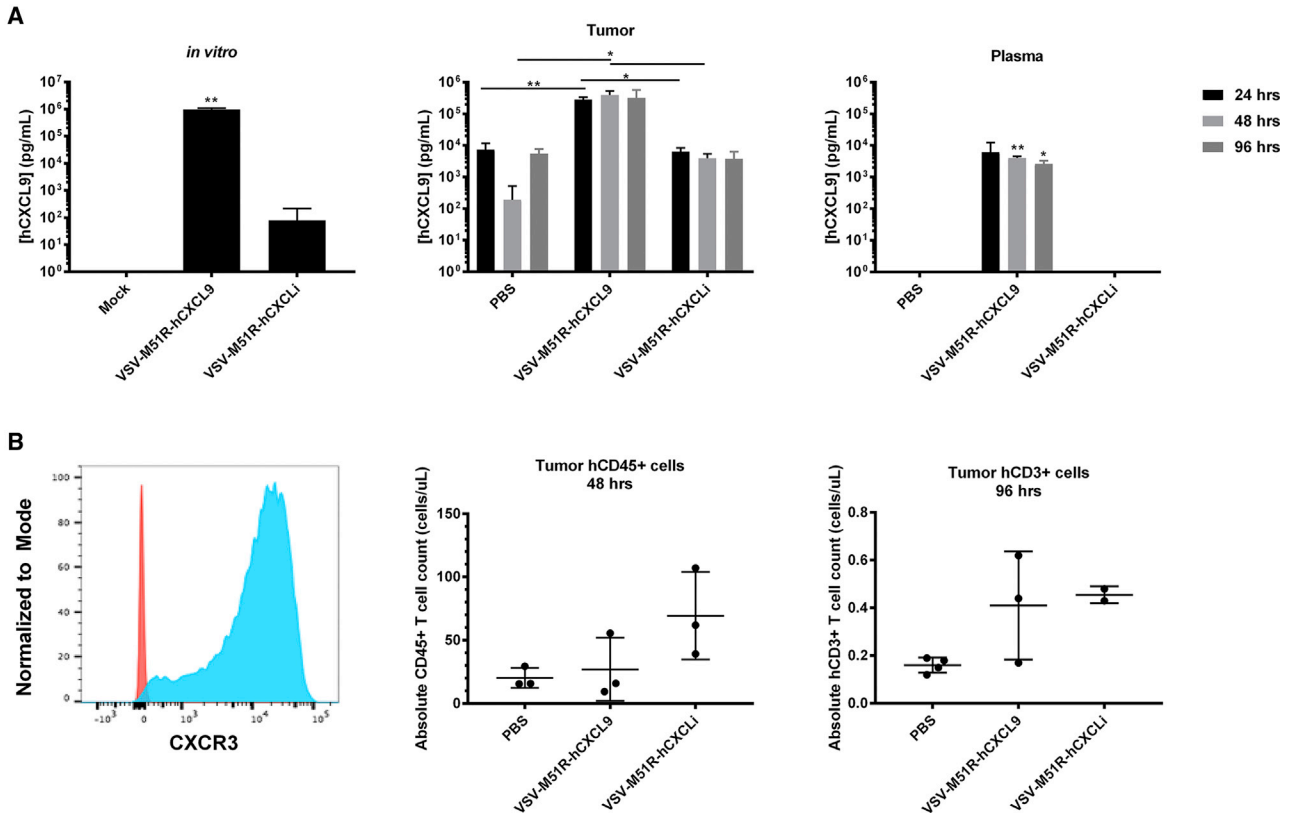

Figure 7. VSV-M51R-hCXCL9 Expresses hCXCL9 Chemokine *In Vitro* and *In Vivo*

(A) Human CXCL9 expression from VSV-M51R-hCXCL9 was tested *in vitro* in FaDu-Luc cells. Supernatants of FaDu-Luc cells were collected 48 h postinfection with VSV-M51R-hCXCL9, VSV-M51R-hCXCLi, (MOI 0.01) or after mock infection, and were assayed by ELISA (first panel). Data are presented as average concentration + standard deviation. Intratumoral and plasma hCXCL9 concentrations at various time points following virus injection were determined in FaDu-Luc tumor-bearing mice by ELISA (n = 3 mice/group for each time point). Values are presented as average chemokine concentration in pg/mL + standard deviation (second and third panels). Significance was determined by t test (*$p < 0.05$, **$p < 0.01$). (B) Human T cells were activated, and CXCR3 expression was tested by flow cytometry. Fluorescence minus one-stained cells are shown in red, and CXCR3-stained cells are shown in blue. FaDu-Luc tumors were harvested and processed 2 and 4 days after intratumoral injection of VSV-M51R-hCXCL9, VSV-M51R-hCXCLi, or PBS treatment (corresponding, respectively, to 1 and 3 days post adoptive T cell transfer). Flow data were gated on live $hCD45^+$ or $hCD3^+$ cells. T cell numbers are presented as average number of immune cells ± standard deviation (n = 3 mice/group for 48 h; n = 4 for PBS treated, n = 3 for VSV-M51R-hCXCL9 treated, and n = 2 for VSV-M51R-hCXCLi at 96 h).

CXCL9-mediated early clearance of VSV is employment of a conditional expression system. A recent report demonstrated that GFP and luciferase reporter gene expression can be controlled by a guanine-responsive riboswitch engineered into VSV.[44] Using this system to time CXCL9 expression following initial VSV replication may improve therapeutic outcomes. Alternatively, encoding CXCL9 into a different OV such as adenovirus or vaccinia, under the control of a tetracycline or cre recombinase conditional expression system, is a direction that warrants future studies.

In conclusion, our study demonstrates that an oncolytic VSV infection can provoke the release of CXCL9 *in vitro* and *in vivo* in multiple tumor models, but suggests that engineering the virus to drive the expression of CXCL9 at supraphysiological levels may have minimal beneficial impact in boosting the recruitment of immune cells into a treated tumor, or in enhancing antitumor efficacy. This study may have important implications for the design and testing of OVs encoding any one of the numerous host proteins involved in the orchestration of an antitumor immune response.

MATERIALS AND METHODS

Cell Culture and Reagents

Baby hamster kidney (BHK) cells, African green monkey kidney cells (Vero), HEK293 T cells, and MPC-11 were maintained in Dulbecco's modified Eagle's medium (DMEM) (catalog number SH30022.01; GE Healthcare Life Sciences), supplemented with 10% fetal bovine serum (FBS) (catalog number 10270106; GIBCO, Life Technologies), at 37°C with 5% CO_2. LM2 cells were a generous gift from Dr. Manish Patel's Laboratory at the University of Minnesota (MN, USA) and were maintained in 10% FBS in Minimal Essential Media (MEM) (catalog number 12561-056; GIBCO, Life Technologies) at 37°C with 5% CO_2. 5TGM1 murine myeloma cells were maintained in

Iscove's Modified Dulbecco's Media (IMDM) (catalog number 12440053; GIBCO, Life Technologies) with 20% FBS at 37°C with 5% CO_2. FaDu-Luc human head and neck carcinoma cells were a generous gift from Dr. Kah Whye Peng's Laboratory at Mayo Clinic (Rochester, MN, USA) and were maintained in DMEM with 10% FBS at 37°C with 5% CO_2.

Lentivirus Transduction of LM2 Cells

mcxcl9 or *gfp* was cloned into the pSIN-CSGW-PKG-puro lentiviral vector plasmid (kindly provided by Dr. Paul Lehner, Cambridge Institute for Medical Research) by utilizing the unique BamHI and XhoI restriction sites. Genes were expressed from the spleen focus-forming virus promoter (SFFV). A total of 4×10^6 HEK293T cells/dish were plated in a 10-cm dish and transfected with lentiviral plasmid, packaging plasmid, and envelope plasmid at a 3:2:1 ratio, respectively, using Fugene-6 (E2691; Promega). Fresh media were added at 18 h, and supernatant was collected 48 h following the addition of fresh media. Lentiviral particles were concentrated down by centrifugation for 90 min at 77,175 relative centrifugal force (RCF) in SW-41Ti rotor. LM2 cells (1×10^5 cells/well) were plated in a 24-well plate and transduced for 48 h at 37°C, then passaged and selected under 3.3 μg/mL puromycin (A1113803; GIBCO) in complete media. The mCXCL9 and GFP stably expressing LM2 cells were used for experiments.

Construction and Generation of VSV Encoding Chemokines

Murine chemokines *cxcl9* and *cxcli* genes were cloned into the VSV-MC11 plasmid between the glycoprotein and large genes.[45] CXCLi had a portion of the CXCR3 receptor binding domain deleted from the *mcxcl9* gene. Mouse *cxcl9* was PCR amplified from a mCXCL9 cloning plasmid (catalog number MG50155-M; Sino Biological, Wayne, PA, USA). CXCL9 forward and reverse primers were designed with AvrII and SbfI restriction sites, respectively. PCR products were run on a 1% agarose gel, and amplicons of the correct size (mCXCL9: 381 bp, murine CXCLi: 351 bp) were cut out and purified using a gel extraction kit (K0692; Thermo Fisher Scientific). PCR products were digested at 37°C for 16 h. Digestions consisted of PCR, AvrII (catalog number R0174S; NEB), SbfI (catalog number R0642S; NEB), and buffer B (BB5; Thermo Fischer Scientific). Primer sequences are as follows: mCXCL9 F AvrII (5′-GGG GGGGGGACCTAGGCCACCATGAAGTCCGCTGTTCTTTT-3′), mCXCL9 R SbfI (5′-GGGGGGGGGACCTGCAGGTTATGTAGT CTTCCTTGAACGA-3′), mCXCL9 mut R (5′-CTGTTTGAGGT CTTTGAGGGATTTGTAGTGGATCGTGCCATTCCTTATCACT AGGGT-3′), and mCXCL9 mut F (5′-GGAGTTCGAGGAACC CTAGTGATAAGGAATGGCACGATCCACTACAAATCCCTCA AA-3′). mCXCLi was produced in two fragments and combined with overlapping PCR with mCXCL9 F AvrII and mCXCL9 R SbfI. The first fragment was amplified with mCXCL9 F AvrII and mCXCL9 mut R primers, and the second fragment was amplified with mCXCL9 mut F and mCXCL9 R SbfI. The coding sequences of *hcxcl9* (GenBank: NM_002416) and *hcxcli* were synthesized with AvrII and SbfI restriction sites flanking the gene and subcloned into the VSV-M51R-MC11 backbone as described above. *hcxcli* had an 11-amino acid deletion (amino acids 27–38) from the human *cxcl10* chemokine corresponding to a portion of the CXCR3 receptor binding domain. Chemokine gene inserts were ligated into pVSV-M51R-MC11 with T4 DNA Ligase (M0202; NEB) at 16°C overnight, transformed into DH5α cells, and purified by miniprep purification (K0502; Thermo Fisher Scientific).

Recombinant VSVs were generated as previously described.[10] In brief, 5×10^5 BHK cells were plated per well in six-well plates. The cells were infected with vaccinia encoding T7 polymerase. After 1 h, vaccinia virus was removed and the cells were transfected with 1 μg of VSV plasmid, 0.5 μg of pN, 0.4 μg of pP, and 0.2 μg of pL all in the pCI vector with FuGENE 6 (E2693; Promega), according to the manufacturer's instructions.[45] The transfection complexes were added dropwise to the wells and incubated at 37°C. Supernatant was removed at 24 h, and complete media were added to the cells. At 70% cytopathic effects (CPEs), supernatant was collected, filtered twice through a 0.22-μm filter, and 1 μL was transferred to freshly plated 2×10^6 Vero cells in a T75 flask. Recombinant VSVs were passaged three times and titrated in Vero cells using the $TCID_{50}$ titration method as previously described.[46] All recombinant viruses were verified by sequence analysis and had low or undetectable endotoxin levels; all stocks had endotoxin concentrations below the acceptable limit for animal studies.

Growth Curve and Viability Analysis

For multistep growth curves, Vero cells were incubated with recombinant VSV at MOIs of 0.1 for VSV-expressing murine chemokines or 0.01 for VSV-expressing human chemokines for 2 h at 37°C in serum-free media. Postincubation, the supernatant was removed, and cells were washed once with PBS, followed by complete media addition. Supernatant was collected at pre-determined time points (2, 8, 12, 24, 31, 48, and 72 h). Virus was titrated in Vero cells using the Spearman Kärber $TCID_{50}$ titration method in 96-well plates. CPE was visually assessed at 72 h postinfection.

Viability assays were performed using yellow tetrazolium (MTT) (30-1010K; ATCC) according to the manufacturer's protocols. In brief, 1×10^4 Vero, LM2, or FaDu-Luc cells were plated in 96-well plates and infected with virus, and 10 μL of MTT reagent was added and incubated at 37°C with 5% CO_2 until purple precipitate was visible (2–4 h). A total of 100 μL of detergent reagent was added, incubated for 2 h at room temperature in the dark, and read at 570 nm. Cell viability is presented as percent viability of mock-infected cells.

ELISA

mCXCL9 and hCXCL9 ELISAs were purchased from RayBiotech (ELM-MIG and ELH-MIG; Peachtree Corners, GA, USA). A total of 5×10^4 LM2 or FaDu-Luc cells were seeded in 24-well plates and incubated for 2 h with VSVs at an MOI of 0.01 or 0.1. Cell culture supernatants were collected from murine and human tumor cells at 24 or 48 h after virus infection, and chemokine concentrations were assayed according to the manufacturer's instructions.

Intratumoral chemokine concentrations were determined by ELISA and processed as follows. Tumors were collected in sterile tubes on

ice, and weights were recorded. Tumors were manually crushed through a 70-μm filter and washed with 1 mL of sterile Dulbecco's PBS (DPBS). Samples were spun down at 1,500 rpm for 5 min at 4°C, and the supernatants were collected and stored at −80°C until analysis. No cell lysis solution was added throughout the processing. Supernatants were diluted in diluent provided by the ELISA kit, and the ELISA was performed according to manufacturers' instructions. In brief, diluted samples and standards were added to the ELISA plate for 2.5 h, washed, and the biotinylated antibody was added for 1 h. The plate was washed again, streptavidin was added for 45 min, and washed. The 3,3′,5,5′-Tetramethylbenzidine (TMB) substrate was added for 30 min, stop solution was added, and the plate was read at 450 nm immediately. Concentrations were determined based on the absorbance values from the standard curve.

T Cell Chemotaxis Assay

Murine T cell migration assays were adapted from what was described previously.[29] In short, spleens from OT-1 mice were collected and processed for cells to be in a single-cell suspension. T cells were activated with SINFEEKL peptide and interleukin-2 (IL-2) for 72 h. Cells were split, supplemented with IL-2 every 2 days after, and collected on days 6–8 for use in migration assays. Supernatants from LM2 cells infected with VSV were used to analyze chemokine functionality. A total cell culture supernatant volume of 33 μL was added to the bottoms of 5-μm Neuroprobe plates (106-5; Gaithersburg, MD, USA). The membrane was placed over the supernatants, and 1×10^4 activated T cells were placed on the top of the membrane. The plate was incubated at 37°C for 2 h, and cells on the bottom well were manually counted via light microscopy.

Primary human T cells were activated with anti-human CD3 and anti-human CD28 beads (#11141D, Dynabeads; Invitrogen) according to the manufacturer's instructions and frozen at −80°C for use in *in vivo* assays.

Animal Studies

All animal studies were approved by Mayo Clinic's Institutional Animal Care and Use Committee (IACUC). Female A/J mice aged 6–8 weeks were ordered from Jackson Laboratories for implantation of LM2 non-small cell lung cancer tumors. Mice were implanted subcutaneously with 1×10^6 cells in 100 μL PBS on the right flank. When tumors reached an average size of 6 mm in diameter, mice were randomized by tumor volume so that the individuals within each group and the group tumor volume average were approximately the same. Mice were treated with a single intratumoral dose of virus administered in 50 μL PBS. Tumor volume was measured via hand-held calipers, and weight was also monitored. Mice were sacrificed at 24 and 96 h for the tumor and serum chemokine study, at 7 and 10 days to evaluate tumor immune infiltration, or when they reached euthanasia criteria for the tumorigenicity and survival studies. Euthanasia criteria included tumor volume greater than 2,000 mm^3, weight loss greater than 10%, clinical signs of neurotoxicity, moribund state, tumor ulceration reaching greater than 50% coverage of the tumor, or mice were unable to access food or water.

Forty male and female C57BL/KaLwRij mice aged 6–8 weeks were implanted subcutaneously with 5×10^6 5TGM1 cells in 100 μl PBS on the right flank. Mice were randomly assigned to treatment groups by tumor volume when tumors measured about 6 mm in length or width, with 9–10 mice per group. VSV and PBS were injected intravenously at a dose of 5×10^7 $TCID_{50}$ in a total volume of 100 μL PBS. Body weights and hand-held caliper tumor measurements were recorded at least two times per week until the study end or until mice reached euthanasia criteria as described above. In contrast with the LM2 model, ulceration was not permitted in this tumor model, and thus acted as an endpoint.

Female NOD scid gamma (NSG) mice aged 6–8 weeks were implanted subcutaneously with 1×10^6 FaDu-Luc cells in 100 μL PBS on the right flank. Mice were randomly assigned to treatment groups by tumor volume when tumors measured about 6 mm in length or width. Mice were euthanized at 24, 48, and 96 h post virus treatment. No animals reached euthanasia criteria before the end of the study.

Tumors were processed for flow cytometry and *in vivo* chemokine analysis as follows. Tumors were collected in sterile tubes on ice, and weights were recorded. Tumors were manually crushed through a 70-μm filter and washed with 1 mL of sterile PBS to create a single-cell suspension. Samples were cleared via centrifugation at 1,500 rpm for 5 min at 4°C, and the supernatants were collected and stored at −80°C until analysis.

Flow Cytometry

Activated primary human T cells were stained for CXCR3 expression with Zombie NIR Fixable Viability dye (423105; BioLegend) and CXCR3 phycoerythrin (PE; 353705; BioLegend). NIR dye was diluted 1:1,000 in PBS, and cells were incubated at room temperature for 20 min in the dark, washed, and subsequently stained for 30 min at 4°C in the dark with anti-human CXCR3 antibody. Samples were analyzed using a CantoX cytometer (BD). Results were gated on the fluorescence minus one (FMO) control.

LM2 tumors were stained with fixable live/dead dye (423105; BioLegend) for 20 min at room temperature. Cells were washed and stained with the following extracellular stains: 1:500 fluorescein isothiocyanate (FITC) anti-mouse CD45 (103108; BioLegend), 1:500 BV421 anti-mouse CD3 (100335; BioLegend), 1:500 PerCP-Cy5.5 anti-mouse CD8α (100734; BioLegend), and 1:500 BV605 anti-mouse CD4 (100451; BioLegend) for 30 min in the dark at 4°C. Cells were fixed and permeabilized using an intracellular staining kit (555028; BD Biosciences) according to the manufacturer's instructions. Intracellular staining was conducted using 1:500 allophycocyanin (APC) anti-mouse IFN-γ (554413; BD), 1:200 PE-Cy7 anti-mouse TNF-α (506324; BioLegend), and 1:100 PE anti-mouse T-bet (561265; BD). All samples were fixed with 4% paraformaldehyde (PFA) prior to analysis on the CantoX cytometer. Gates were set based on FMO controls.

FaDu-Luc tumors were stained with fixable live/dead dye for 20 min at room temperature. Cells were washed and stained with 2.5 μL

BV421 anti-human CD45 (304032; BioLegend) or 1.25 μL PE-Cy7 anti-human CD3 (317334; BioLegend) extracellular stains and fixed with 4% PFA before running on the CantoX cytometer with the same protocol as described above.

Statistical Analyses

GraphPad Prism (San Diego, CA, USA) was used to analyze all results. Paired two-tailed t test was used to determine significance of all *in vitro* results, including MTT assays, ELISAs, migration assays, and *in vivo* ELISA, and flow cytometry results. Survival curves were plotted using Kaplan-Meier curves, and log rank (Mantel-Cox) test was used to determine percent survival significance. Tumor sizes were analyzed using a two-way ANOVA with Tukey correction for multiple comparisons.

AUTHOR CONTRIBUTIONS

E.C.E. and S.J.R. conceived the project. E.C.E. conducted the *in vitro* experiments. E.C.E. and R.A.N. performed the *in vivo* experiments. J.M.T. produced the lentiviruses. L.E. contributed to the flow cytometry design and analysis. R.G.V. contributed to the experimental design. E.C.E. and S.J.R. designed the experiments, performed data analysis, and wrote the paper. S.J.R. supervised the project.

CONFLICTS OF INTEREST

S.J.R. is chief executive officer at Vyriad. S.J.R. and Mayo Clinic hold equity in Vyriad.

ACKNOWLEDGMENTS

LM2 cells were a kind gift from Manish Patel at the University of Minnesota. Activated non-transduced primary T cells were graciously provided by Leo Sakemura from the Laboratory of Saad Kenderian at the Mayo Clinic Rochester. The Mayo Microscopy and Cell Analysis Core was utilized for some of the experiments performed in this report, specifically the flow cytometry experiments. This publication was supported by Grant Number UL1 TR002377 from the National Center for Advancing Translational Sciences (NCATS) and CTSA Grant Number TL1 TR002380 from NCATS. Its contents are solely the responsibility of the authors and do not necessarily represent the official views of the NIH.

REFERENCES

1. Griffith, J.W., Sokol, C.L., and Luster, A.D. (2014). Chemokines and chemokine receptors: positioning cells for host defense and immunity. Annu. Rev. Immunol. *32*, 659–702.

2. Barreira da Silva, R., Laird, M.E., Yatim, N., Fiette, L., Ingersoll, M.A., and Albert, M.L. (2015). Dipeptidylpeptidase 4 inhibition enhances lymphocyte trafficking, improving both naturally occurring tumor immunity and immunotherapy. Nat. Immunol. *16*, 850–858.

3. Juric, V., O'Sullivan, C., Stefanutti, E., Kovalenko, M., Greenstein, A., Barry-Hamilton, V., Mikaelian, I., Degenhardt, J., Yue, P., Smith, V., and Mikels-Vigdal, A. (2018). MMP-9 inhibition promotes anti-tumor immunity through disruption of biochemical and physical barriers to T-cell trafficking to tumors. PLoS ONE *13*, e0207255.

4. Nishina, S., Yamauchi, A., Kawaguchi, T., Kaku, K., Goto, M., Sasaki, K., Hara, Y., Tomiyama, Y., Kuribayashi, F., Torimura, T., and Hino, K. (2018). Dipeptidyl peptidase 4 inhibitors reduce hepatocellular carcinoma by activating lymphocyte chemotaxis in mice. Cell. Mol. Gastroenterol. Hepatol. *7*, 115–134.

5. Hollande, C., Boussier, J., Ziai, J., Nozawa, T., Bondet, V., Phung, W., Lu, B., Duffy, D., Paradis, V., Mallet, V., et al. (2019). Inhibition of the dipeptidyl peptidase DPP4 (CD26) reveals IL-33-dependent eosinophil-mediated control of tumor growth. Nat. Immunol. *20*, 257–264.

6. Rainczuk, A., Rao, J.R., Gathercole, J.L., Fairweather, N.J., Chu, S., Masadah, R., Jobling, T.W., Deb-Choudhury, S., Dyer, J., and Stephens, A.N. (2014). Evidence for the antagonistic form of CXC-motif chemokine CXCL10 in serous epithelial ovarian tumours. Int. J. Cancer *134*, 530–541.

7. Peng, D., Kryczek, I., Nagarsheth, N., Zhao, L., Wei, S., Wang, W., Sun, Y., Zhao, E., Vatan, L., Szeliga, W., et al. (2015). Epigenetic silencing of TH1-type chemokines shapes tumour immunity and immunotherapy. Nature *527*, 249–253.

8. Zheng, H., Zhao, W., Yan, C., Watson, C.C., Massengill, M., Xie, M., Massengill, C., Noyes, D.R., Martinez, G.V., Afzal, R., et al. (2016). HDAC inhibitors enhance T-Cell chemokine expression and augment response to PD-1 immunotherapy in lung adenocarcinoma. Clin. Cancer Res. *22*, 4119–4132.

9. Russell, S.J., Peng, K.W., and Bell, J.C. (2012). Oncolytic virotherapy. Nat. Biotechnol. *30*, 658–670.

10. Lawson, N.D., Stillman, E.A., Whitt, M.A., and Rose, J.K. (1995). Recombinant vesicular stomatitis viruses from DNA. Proc. Natl. Acad. Sci. USA *92*, 4477–4481.

11. Zhang, L., Steele, M.B., Jenks, N., Grell, J., Suksanpaisan, L., Naik, S., Federspiel, M.J., Lacy, M.Q., Russell, S.J., and Peng, K.W. (2016). Safety Studies in Tumor and Non-Tumor-Bearing Mice in Support of Clinical Trials Using Oncolytic VSV-IFNβ-NIS. Hum. Gene Ther. Clin. Dev. *27*, 111–122.

12. Naik, S., Galyon, G.D., Jenks, N.J., Steele, M.B., Miller, A.C., Allstadt, S.D., Suksanpaisan, L., Peng, K.W., Federspiel, M.J., Russell, S.J., and LeBlanc, A.K. (2018). Comparative Oncology Evaluation of Intravenous Recombinant Oncolytic Vesicular Stomatitis Virus Therapy in Spontaneous Canine Cancer. Mol. Cancer Ther. *17*, 316–326.

13. Velazquez-Salinas, L., Naik, S., Pauszek, S.J., Peng, K.W., Russell, S.J., and Rodriguez, L.L. (2017). Oncolytic Recombinant Vesicular Stomatitis Virus (VSV) Is Nonpathogenic and Nontransmissible in Pigs, a Natural Host of VSV. Hum. Gene Ther. Clin. Dev. *28*, 108–115.

14. Naik, S., Nace, R., Federspiel, M.J., Barber, G.N., Peng, K.W., and Russell, S.J. (2012). Curative one-shot systemic virotherapy in murine myeloma. Leukemia *26*, 1870–1878.

15. Patel, M.R., Jacobson, B.A., Ji, Y., Drees, J., Tang, S., Xiong, K., Wang, H., Prigge, J.E., Dash, A.S., Kratzke, A.K., et al. (2015). Vesicular stomatitis virus expressing interferon-β is oncolytic and promotes antitumor immune responses in a syngeneic murine model of non-small cell lung cancer. Oncotarget *6*, 33165–33177.

16. Chow, M.T., Ozga, A.J., Servis, R.L., Frederick, D.T., Lo, J.A., Fisher, D.E., Freeman, G.J., Boland, G.M., and Luster, A.D. (2019). Intratumoral Activity of the CXCR3 Chemokine System Is Required for the Efficacy of Anti-PD-1 Therapy. Immunity *50*, 1498–1512.e5.

17. Pan, J., Burdick, M.D., Belperio, J.A., Xue, Y.Y., Gerard, C., Sharma, S., Dubinett, S.M., and Strieter, R.M. (2006). CXCR3/CXCR3 ligand biological axis impairs RENCA tumor growth by a mechanism of immunoangiostasis. J. Immunol. *176*, 1456–1464.

18. Wu, Z., Huang, X., Han, X., Li, Z., Zhu, Q., Yan, J., Yu, S., Jin, Z., Wang, Z., Zheng, Q., and Wang, Y. (2016). The chemokine CXCL9 expression is associated with better prognosis for colorectal carcinoma patients. Biomed. Pharmacother. *78*, 8–13.

19. Cao, Y., Huang, H., Wang, Z., and Zhang, G. (2017). The Inflammatory CXC Chemokines, GROα^{high}, IP-10^{low}, and MIG^{low}, in Tumor Microenvironment Can Be Used as New Indicators for Non-small Cell Lung Cancer Progression. Immunol. Invest. *46*, 361–374.

20. Ohtani, H., Jin, Z., Takegawa, S., Nakayama, T., and Yoshie, O. (2009). Abundant expression of CXCL9 (MIG) by stromal cells that include dendritic cells and accumulation of CXCR3+ T cells in lymphocyte-rich gastric carcinoma. J. Pathol. *217*, 21–31.

21. Mulligan, A.M., Raitman, I., Feeley, L., Pinnaduwage, D., Nguyen, L.T., O'Malley, F.P., Ohashi, P.S., and Andrulis, I.L. (2013). Tumoral lymphocytic infiltration and expression of the chemokine CXCL10 in breast cancers from the Ontario Familial Breast Cancer Registry. Clin. Cancer Res. *19*, 336–346.

22. Hensbergen, P.J., Wijnands, P.G., Schreurs, M.W., Scheper, R.J., Willemze, R., and Tensen, C.P. (2005). The CXCR3 targeting chemokine CXCL11 has potent antitumor activity *in vivo* involving attraction of CD8+ T lymphocytes but not inhibition of angiogenesis. J. Immunother. *28*, 343–351.

23. K Au, K., Peterson, N., Truesdell, P., Reid-Schachter, G., Khalaj, K., Ren, R., Francis, J.A., Graham, C.H., Craig, A.W., and Koti, M. (2017). CXCL10 alters the tumour immune microenvironment and disease progression in a syngeneic murine model of high-grade serous ovarian cancer. Gynecol. Oncol. *145*, 436–445.

24. Karin, N., and Wildbaum, G. (2015). The role of chemokines in adjusting the balance between CD4+ effector T cell subsets and FOXp3-negative regulatory T cells. Int. Immunopharmacol. *28*, 829–835.

25. Liao, F., Rabin, R.L., Yannelli, J.R., Koniaris, L.G., Vanguri, P., and Farber, J.M. (1995). Human Mig chemokine: biochemical and functional characterization. J. Exp. Med. *182*, 1301–1314.

26. Vanheule, V., Janssens, R., Boff, D., Kitic, N., Berghmans, N., Ronsse, I., Kungl, A.J., Amaral, F.A., Teixeira, M.M., Van Damme, J., et al. (2015). The Positively Charged COOH-terminal Glycosaminoglycan-binding CXCL9(74-103) Peptide Inhibits CXCL8-induced Neutrophil Extravasation and Monosodium Urate Crystal-induced Gout in Mice. J. Biol. Chem. *290*, 21292–21304.

27. Mlecnik, B., Tosolini, M., Charoentong, P., Kirilovsky, A., Bindea, G., Berger, A., Camus, M., Gillard, M., Bruneval, P., Fridman, W.H., et al. (2010). Biomolecular network reconstruction identifies T-cell homing factors associated with survival in colorectal cancer. Gastroenterology *138*, 1429–1440.

28. Stojdl, D.F., Lichty, B.D., tenOever, B.R., Paterson, J.M., Power, A.T., Knowles, S., Marius, R., Reynard, J., Poliquin, L., Atkins, H., et al. (2003). VSV strains with defects in their ability to shutdown innate immunity are potent systemic anti-cancer agents. Cancer Cell *4*, 263–275.

29. Campanella, G.S.V., Medoff, B.D., Manice, L.A., Colvin, R.A., and Luster, A.D. (2008). Development of a novel chemokine-mediated in vivo T cell recruitment assay. J. Immunol. Methods *331*, 127–139.

30. Heissmeyer, V., Macián, F., Im, S.H., Varma, R., Feske, S., Venuprasad, K., Gu, H., Liu, Y.C., Dustin, M.L., and Rao, A. (2004). Calcineurin imposes T cell unresponsiveness through targeted proteolysis of signaling proteins. Nat. Immunol. *5*, 255–265.

31. Adachi, Y., Hattori, M., and Yoshida, T. (2010). Regulation of T cell activation and anergy by the intensity of the Ca^2+ signal in cooperation with other signals. Biosci. Biotechnol. Biochem. *74*, 1788–1793.

32. Moon, E.K., Wang, L.S., Bekdache, K., Lynn, R.C., Lo, A., Thorne, S.H., and Albelda, S.M. (2018). Intra-tumoral delivery of CXCL11 via a vaccinia virus, but not by modified T cells, enhances the efficacy of adoptive T cell therapy and vaccines. OncoImmunology *7*, e1395997.

33. Li, H., Peng, K.W., and Russell, S.J. (2012). Oncolytic measles virus encoding thyroidal sodium iodide symporter for squamous cell cancer of the head and neck radiovirotherapy. Hum. Gene Ther. *23*, 295–301.

34. Patel, M.R., Dash, A., Jacobson, B.A., Ji, Y., Baumann, D., Ismail, K., and Kratzke, R.A. (2019). JAK/STAT inhibition with ruxolitinib enhances oncolytic virotherapy in non-small cell lung cancer models. Cancer Gene Ther. *26*, 411–418.

35. Rosewell Shaw, A., Porter, C.E., Watanabe, N., Tanoue, K., Sikora, A., Gottschalk, S., Brenner, M.K., and Suzuki, M. (2017). Adenovirotherapy Delivering Cytokine and Checkpoint Inhibitor Augments CAR T Cells against Metastatic Head and Neck Cancer. Mol. Ther. *25*, 2440–2451.

36. Maroun, J., Muñoz-Alía, M., Ammayappan, A., Schulze, A., Peng, K.W., and Russell, S. (2017). Designing and building oncolytic viruses. Future Virol. *12*, 193–213.

37. Tognarelli, E.I., Palomino, T.F., Corrales, N., Bueno, S.M., Kalergis, A.M., and González, P.A. (2019). Herpes Simplex Virus Evasion of Early Host Antiviral Responses. Front. Cell. Infect. Microbiol. *9*, 127.

38. Su, C., Zhan, G., and Zheng, C. (2016). Evasion of host antiviral innate immunity by HSV-1, an update. Virol. J. *13*, 38.

39. Smith, G.L., Benfield, C.T., Maluquer de Motes, C., Mazzon, M., Ember, S.W., Ferguson, B.J., and Sumner, R.P. (2013). Vaccinia virus immune evasion: mechanisms, virulence and immunogenicity. J. Gen. Virol. *94*, 2367–2392.

40. Perdiguero, B., and Esteban, M. (2009). The interferon system and vaccinia virus evasion mechanisms. J. Interferon Cytokine Res. *29*, 581–598.

41. Liu, Z., Ravindranathan, R., Li, J., Kalinski, P., Guo, Z.S., and Bartlett, D.L. (2015). CXCL11-Armed oncolytic poxvirus elicits potent antitumor immunity and shows enhanced therapeutic efficacy. OncoImmunology *5*, e1091554.

42. Francis, L., Guo, Z.S., Liu, Z., Ravindranathan, R., Urban, J.A., Sathaiah, M., Magge, D., Kalinski, P., and Bartlett, D.L. (2016). Modulation of chemokines in the tumor microenvironment enhances oncolytic virotherapy for colorectal cancer. Oncotarget *7*, 22174–22185.

43. Liu, Z., Ravindranathan, R., Kalinski, P., Guo, Z.S., and Bartlett, D.L. (2017). Rational combination of oncolytic vaccinia virus and PD-L1 blockade works synergistically to enhance therapeutic efficacy. Nat. Commun. *8*, 14754.

44. Takahashi, K., and Yokobayashi, Y. (2019). Reversible Gene Regulation in Mammalian Cells Using Riboswitch-Engineered Vesicular Stomatitis Virus Vector. ACS Synth. Biol. *8*, 1976–1982.

45. Ammayappan, A., Nace, R., Peng, K.W., and Russell, S.J. (2013). Neuroattenuation of vesicular stomatitis virus through picornaviral internal ribosome entry sites. J. Virol. *87*, 3217–3228.

46. Ruiz, A.J., Hadac, E.M., Nace, R.A., and Russell, S.J. (2016). MicroRNA-Detargeted Mengovirus for Oncolytic Virotherapy. J. Virol. *90*, 4078–4092.